HHS Public Access

Author manuscript

Exp Lung Res. Author manuscript; available in PMC 2020 September 01.

Published in final edited form as:

Exp Lung Res. 2019 September ; 45(7): 175–187. doi:10.1080/01902148.2019.1636899.

Restrictive lung disease in TNF-transgenic mice: correlation of pulmonary function testing and micro-CT imaging

Emily K. Wu[1,2], **Sophia Eliseeva**[1], **Homaira Rahimi**[2,3], **Edward M. Schwarz**[2,4], **Steve N. Georas**[1,5]

[1]Department of Microbiology and Immunology..University of Rochester School of Medicine and Dentistry, Rochester, NY

[2]Center for Musculoskeletal Research, University of Rochester School of Medicine and Dentistry, Rochester, NY

[3]Department of Pediatrics, University of Rochester School of Medicine and Dentistry, Rochester, NY

[4]Department of Orthopaedics, University of Rochester School of Medicine and Dentistry, Rochester, NY

[5]Division of Pulmonary and Critical Care Medicine, Department of Medicine, University of Rochester School of Medicine and Dentistry, Rochester, New York

Abstract

Purpose: Micro-computed tomography (μCT) is increasingly being used on animal models as a minimally-invasive longitudinal outcome measure of pulmonary disease progression. However, while imaging can elucidate macroscopic structural changes over the whole lung, μCT is unable to describe the mechanical changes and functional impairments imposed by progressive disease, which can only be measured via pulmonary function tests (PFTs). The tumor necrosis factor-transgenic (TNF-Tg) mouse model of rheumatoid arthritis (RA) develops pulmonary pathology that mimics many aspects of the inflammatory interstitial lung disease (ILD) seen in a subset of patients with RA. Prior studies using μCT imaging of these mice found increased pulmonary density, characteristic of restrictive disease; however, there have been conflicting reports in the literature regarding the obstructive versus restrictive phenotype of this model. Our study looks to 1) define the functional impairments and 2) characterize the restrictive/obstructive nature of the disease found in this model.

Materials and Methods: In this study, we performed PFTs at end-stage ILD, and paired these findings with μCT results, correlating radiology to functional parameters. TNF-Tg and WT littermates of both sexes underwent μCT imaging and PFT testing at 5.5 months-old. Spearman's correlation analyses were performed comparing lung tissue volume (LTV) to PFT parameters of gas exchange and tissue stiffness.

Corresponding Author: Steve N. Georas, MD, Address: 601 Elmwood Ave, University of Rochester Medical Center Division of Pulmonary & Critical Care Medicine, Rochester, NY 14642, Phone: (585) 275-4861, Fax: (585) 273-1114, steve_georas@urmc.rochester.edu.

Author Contributions: Conception and design—E.K.W., E.M.S., and S.N.G.; performed experiments—E.K.W. and S.E.; data analysis—E.K.W.; results interpretation—E.K.W., H.R., E.M.S., and S.N.G.; drafting the manuscript—E.K.W. and S.N.G.

Results: Compared to WT, TNF-Tg mice had impaired gas exchange capacity, increased respiratory resistance, and reduced lung compliance, elastance, and inspiratory capacity, indicating increased tissue stiffness and compromised pulmonary function. LTV was also consistently higher in TNF-Tg lungs.

Conclusions: These findings demonstrate that: 1) TNF-Tg mice display a restrictive pathology, and 2) in vivo μCT is a valid outcome measure to infer changes in pulmonary mechanical and functional parameters.

Keywords

micro-CT; pulmonary function testing; rheumatoid arthritis-associated interstitial lung disease; TNF-transgenic

Introduction

Interstitial lung disease (ILD) is one of the leading causes of morbidity and mortality in rheumatoid arthritis (RA) patients (1–5). In fact, it is estimated that patients with RA have a 10% lifetime risk of being diagnosed with ILD (3). Patients with RA-associated ILD (RA-ILD) develop a restrictive pulmonary disease with either an inflammatory pathology rooted in cellular infiltration, or a predominantly fibrotic pathology with elements of inflammatory change (6–8). Clinically, these phenotypes are broken down into different subtypes of ILD based on histopathology and chest CT imaging studies. Of these, the majority of RA-ILD cases are classified as either usual interstitial pneumonia (UIP) or non-specific interstitial pneumonia (NSIP) (3, 9–12). UIP is defined as being largely fibrotic in nature, predominated by dense areas of collagen deposition, while NSIP contains more inflammatory components with diffuse cellular infiltration and less significant fibrotic activity (13).

Clinically, physicians rely on high-resolution computed tomography (HRCT) imaging to diagnose and assess RA-ILD cases. Based on the known disease course of ILD pathologies, patients with RA often demonstrate initial signs of pulmonary pathology on imaging prior to developing symptomatic disease, subsequently leading to diagnosis. In this capacity, HRCT scans have replaced lung biopsies as the preferred mode of diagnosis, based on correlations between histologic changes and imaging patterns. Following the initial diagnosis, HRCT imaging is routinely used as a non-invasive way to assess disease progression.

In the context of pre-clinical studies, micro-computed tomography (μCT) is being increasingly applied to mouse models of pulmonary disease (14–17). While ex vivo outcome measures are still the most commonly used methods for analyzing experimental models of pulmonary disease, the benefits of μCT imaging as a non-invasive and longitudinal evaluation tool to follow disease development and progression are being increasingly recognized. As a relatively new technique for use in murine models, μCT has mostly been used in the context of pulmonary fibrosis (15, 16). We believe that μCT has the potential for more widespread usage in evaluating multiple models of pulmonary diseases, including interstitial lung disease.

Pulmonary function tests (PFTs) are also routinely used in clinical settings to diagnose and follow the progression of lung disease in patients with RA-ILD, and certain parameters have been found to be associated with disease outcome (18, 19). By measuring flow rates, lung volumes, and gas exchange, PFTs provide the foundation for assessing disease pathophysiology. Patients with RA-ILD typically develop restrictive lung disease, characterized by reductions in lung volumes without evidence of airflow limitation. Another common manifestation of RA-ILD is a reduced diffusing capacity, reflecting decreased lung surface area available for gas exchange. The combination of lung restriction with decreased diffusing capacity results in significant functional impairment as RA-ILD progresses (20). In a similar manner to HRCTs, PFTs are embraced in the clinic as both non-invasive and cost-effective methods of disease assessment. However, HRCT scans have been shown to detect smaller pathologic patterns in the tissue at earlier stages of disease development compared to PFTs (21).

Despite the convenience of PFT evaluations in clinical settings, PFT testing is far more limiting in the context of animal models. In mouse models, accurate measurement of PFTs typically involves the placement of a tracheostomy and paralysis of the thoracic muscles to limit voluntary respiration (22, 23). Although some lung function measurements can be obtained in non-restrained or spontaneously breathing mice, comprehensive lung function testing is usually a terminal experiment, which limits their use in following disease progression longitudinally in animal models. The idea of associating a non-invasive measure such as μCT with changes in PFT outcomes has been expressed, but the existing data is preliminary and not very extensive (17).

Our lab has been studying the tumor necrosis factor-transgenic (TNF-Tg) mouse model of RA, in which the human TNF-α gene is overexpressed (24, 25). In addition to its more rigorously characterized joint pathology, the 3647 TNF-Tg mouse line manifests an inflammatory lung phenotype and has been utilized as a model of RA-ILD (25–27). Multiple TNF-Tg models exist which vary based on pathologic severity and mechanism of TNF-α overexpression. Depending on the specific line, TNF-Tg mice can also develop varying degrees of lung fibrosis or emphysema (28, 29). Moreover, we previously validated μCT imaging for use in the TNF-Tg mouse against histopathologic parameters for assessment of pulmonary disease (14). Using 3D- μCT scanning and volumetric reconstruction of the lungs, it was found that lung tissue volume was significantly increased in TNF-Tg mice when compared to their WT littermate counterparts. While the evidence of increased pulmonary density supports the assessment of restrictive disease in the model, further evaluation regarding the nature of the pathology is limited by resolution restrictions, which prevent us from delineating specific imaging patterns.

Further histologic evaluation of other TNF-mediated lung models reveals several classic features of an inflammatory ILD. However, evidence from multiple models of TNF-α overexpression have presented signs of pathologic components which would make the TNF-Tg an inaccurate model for a purely restrictive-like lung disease, citing emphysematous changes on histology (28, 29). Despite the conclusions that can be inferred from μCT imaging data, how these relate to a restrictive or obstructive pulmonary pathophysiology is not clear. Given the reproducible nature of the 3547 line TNF-Tg, along with the prior

correlations made between μCT data and histologic quantification data, we hypothesized that μCT data also directly correlates with functional and mechanical parameters of lung physiology. Using pulmonary function testing and μCT scanning, we have: 1) evaluated the physiologic and mechanical properties of TNF-Tg lungs to assess the validity of this model for RA-ILD, and 2) validated μCT as a minimally invasive outcome measure for longitudinal assessment of pulmonary disease in murine models.

Methods

Animals

The 3647 line of the TNF-transgenic (TNF-Tg) mouse model on a C57BL/6 background was originally obtained from Dr. G. Kollias (University of Athens). Male and female TNF-Tg mice with WT littermates were used (n=6 per cohort) at 5.5 months of age. Mice were dosed with 100 mg/kg ketamine + 10 mg/kg xylazine administered IP for anesthesia, and with 1.3 mg/kg Vencuronium for paralytic purposes in compliance with UCAR policy. All experiments were conducted in compliance with the University of Rochester Medical Center University Committee on Animal Resources (UCAR) policies.

Micro-computed tomography (μCT)

Cross-sectional μCT imaging was performed on all mice as listed above. Mice were anesthetized using 1.5–2% isofluorane and placed into a vivaCT 40 μCT machine (Scanco Medical, Bruttisellen, Switzerland). The mice were placed in a central compartment in the pronated position over a blood-pressure transducer (BPS-BTA and SDAQ, Vernier, Beaverton OR) for the purposes of monitoring the respiratory cycle via chest wall movements. Respiratory gating via LabVIEW (National Instruments, Austin, Texas, USA) was used to selectively image the lungs in the post-exhalation period of the respiratory cycle to minimize movement artifacts. DICOMs at 35 μm^3 isotropic voxel resolution were imported to Amira (FEI, Hillsboro, Oregon, USA) for semi-automated segmentation. μCT parameters and analysis via Amira software as previously described (14) were used for image collection, analysis, and 3-dimensional rendering.

Gas Chromatography

Gas chromatography (GC) was performed on male and female TNF-Tg and WT cohorts (n=6 per cohort) using a Micro GC Fusion instrument (Micro GC Fusion, INFICON, Basel, Switzerland) to measure lung diffusion capacity. Adult (5.5-month-old) mice were anesthetized with ketamine/xylazine and tracheostomized via a 19-guage blunt tip cannula. After cannulation, the mice were placed on a warming mattress and the lungs were inflated for 9 seconds with 0.8 mL of a specific gaseous cocktail containing 0.3% carbon monoxide and 0.5% neon gas with ultra-pure helium as the carrier gas. 0.8 mL of gas was then extracted from the lung and diluted with 1.2 mL of room air prior to the administration of the full 2 mL into the gas chromatograph. Each sample was done in duplicate, with two inflations and readings per mouse. Mice were allowed to breathe freely in between inflations. After the two manipulations, mice were taken directly for mechanical testing. Results were analyzed as a measure of the diffusion factor for carbon monoxide (DFCO), calculated as $DFCO=1-((CO_9/Ne_9)/(CO_c/Ne_c))$ as previously reported (22, 30). The c and 9

subscripts refer to the concentrations of each gas at calibration and post-9 second inhalation, respectively. The DFCO parameter therefore describes the concentrations of gas at "exhalation" normalized to the known calibration concentrations of gaseous components at "inhalation".

Pulmonary Function Testing

Mechanical testing was performed with the use of the flexiVent (SCIREQ Scientific Respiratory Equipment Inc, Montreal, Quebec, Canada) on each mouse immediately following GC evaluation. Mice were continuously anesthetized with the previously administered ketamine/xylazine, and subsequently dosed with Vencuronium (1.3 mg/kg) as a paralytic to ensure the mouse was passive and had no spontaneous or independent breathing movements during experimentation. The mice were kept warm through the duration of the experiment. The cannula previously inserted as a tracheostomy for the GC remained in place and was attached to a small animal mechanical ventilator and respiratory mechanics analyzer (the flexiVent) for further manipulation. The flexiVent then mechanically ventilated the mouse with an estimated tidal volume of 10 mL/kg of room air at 10 breaths/min, PEEP of 3 cmH2O, and FIO2 of 21–50%. Heart rates were monitored via EKG throughout the entire ventilation procedure. The flexiVent then conducted a series of manipulations in the ventilation of the mouse by controlling the rate, volume, and pressure of air forced through the tracheostomy into the mouse. Under the "Deep Inflation" protocol, the lungs were inflated to a pressure of 30 cmH2O over a period of 3 seconds and held at that pressure for another 3 seconds, allowing for the direct calculation of the total inspiratory capacity of the mouse lungs. Following this, a "SnapShot" maneuver involving a single forced oscillation at 2.5 Hz was used to evaluate total respiratory resistance (R_{rs}), elastance (E_{rs}), and compliance (C_{rs}), which includes contributions from the peripheral lung, chest wall, and upper airway. A "Quick Prime" evaluation involving a series of complex forced oscillations allowed for the calculation of Newtonian resistance (R_N), tissue dampening (G), and tissue elastance (H). In the final evaluation, a pressure-volume curve was generated, allowing for the calculation of static compliance (C_{st}), and the shape constant (k). Each mouse was done in triplicate, with three "rounds" of forced ventilatory manipulations performed on each mouse in rapid succession. An average of the three repeated measures for each parameter were calculated and depicted per mouse. After mechanical testing, mice were euthanized with ketamine (300 mg/kg) followed by cervical dislocation in compliance with UCAR protocols.

Histology

Historic lung samples were taken from age-matched mice and stained for histology. The lungs were previously collected at time of tissue harvest via inflation fixation. At harvest, the thoracic cavity was exposed, and 4–0 suture was loosely tied around the trachea. A 27-gauge needle was used to push 10% NBF from a 5 mL syringe into the trachea. Forceps were used to clamp the trachea during the injection. The suture was tightened immediately post-injection to maintain inflation of the lobes. The lungs were then fixed for 3 days in 10% NBF and were processed and embedded in paraffin blocks by the URMC CMSR Histology Core Facility. Lungs underwent coronal sectioning from paraffin in 3 consecutive regions, each 100 μm apart. Each region was ~100 μm thick, each sectioned into a series of 5 μm

slices. Representative slices from each section were stained with Masson's trichrome for evaluation of collagen deposition.

Statistical Analysis

All statistical analyses were performed on Graphpad Prism 7 (GraphPad Software, San Diego, CA). 2-way ANOVA tests with Sidak's post-hoc tests for multiple comparisons were performed on all continuous data sets to examine the effects of genotype (WT vs TNF-Tg), and sex (female vs male). Statistical analyses were considered significant with $p<0.05$. Correlation analyses evaluating the relationship between lung tissue volume (from the μCT) and various functional and mechanical parameters (as measured through gas chromatography and PFTs) were performed using Spearman's rank correlations on the raw data for all parameters.

Results

Pulmonary Gas Exchange is impaired in TNF-Tg mice

Gas chromatography (GC) tests were performed on each mouse to determine pulmonary functional impairment via changes in gas exchange in the lung. Gross differences in body habitus between the genotypes for both sexes were noted as a confirmation of previously noted data (31). Further DFCO calculations show a clear disparity between genotypes, in which TNF-Tg mice are significantly impaired compared to their WT counterparts (WT vs TNF-Tg, females, $p<0.0001$; males, $p=0.0001$) (Fig. 1). Notably, DFCO values have no statistically significant differences between the sexes in TNF-Tg mice (DFCO = 0.3390±0.1058 vs. 0.4425±0.1086 in female vs. male TNF-Tg mice, $p=0.1362$).

TNF-Tg mice demonstrate restrictive pulmonary physiology

We next comprehensively analyzed pulmonary function in WT and TNF-Tg mice using direct measurements of airflow with forced oscillation in sedated and paralyzed mice (see Methods). Total respiratory resistance (R_{rs}), which comprises the resistance to lung expansion by the chest wall, large conducting airways, and peripheral pulmonary tissue, found increased resistance in TNF-Tg animals, most notably in the female cohorts (WT vs TNF-Tg, females, $p=0.0266$; males, $p=0.1745$) (Fig. 2A). Corresponding values of Newtonian resistance (R_N) and tissue dampening (G) allow for more specific analysis regarding the resistance of the large conducting airways and of the peripheral pulmonary tissue, respectively (32). While no significant differences were found between genotypes with regards to R_N (WT vs TNF-Tg, females, $p=0.3949$, males, $p=0.9534$), differences in G indicate an increased pressure per unit volume for TNF-Tg animals as compared to their WT counterparts, which were statistically significant when comparing female mice ($p=0.0129$), but not male mice ($p=0.1597$). These results indicated that small airways and peripheral tissues were the primary contributor to increased total pulmonary resistance, as opposed to the large airways in TNF-Tg mice (Fig. 2B and C). It should be noted that the predominance of these pulmonary function differences were observed in female mice, as opposed to their male counterparts.

Measures of distensibility, including total respiratory compliance (C_{rs}) and elastance (E_{rs}), also revealed similar trends regarding the restrictive physiology of TNF-Tg animals compared to their WT littermate counterparts in which females had greater impairment compared to WT controls than their male counterparts (C_{rs}, WT vs TNF-Tg, females, $p<0.0001$, males, $p=0.0339$) (E_{rs}, WT vs TNF-Tg, females, $p=0.0099$, males, $p=0.2374$) (Fig. 2D and G). Further specificity regarding the contributions from the intrinsic elastic energy stored in the pulmonary tissue (tissue elastance, H) and the elastic properties of the chest wall and pulmonary tissue (static compliance, C_{st}) indicated that changes in peripheral tissues were the dominant contributor to the restrictive physiology of the lung (H, WT vs TNF-Tg, females, $p=0.0244$, males, $p=0.3982$) (C_{st}, WT vs TNF-Tg, females, $p=0.0003$, males, $p=0.0110$) (Fig. 2E and H). Despite the fact that genotype has a more profound influence in the female population, no measures of lung stiffness demonstrated any sexual dimorphism in diseased animals.

The shape constant (k), as derived from pressure-volume curves, describes a volume-independent relationship of pressure changes over the course of a complete respiratory cycle. The decrease in k for both sexes similarly implies a restrictive change in the pulmonary physiology of TNF-Tg mice (Fig. 2F).

Finally, the forced manipulations involved in PFT testing allow for the determination of air volume with full distension of the lung. The total inspiratory capacity (IC) of the lung was found to be significantly decreased for female TNF-Tg mice (Fig. 2I). Taken together, results of comprehensive pulmonary function testing in our model uncovered a significant decrease in gas exchange and lung capacity, driven by changes in the peripheral lung.

It should be noted that analysis regarding sexually dimorphic differences in mechanical properties demonstrated trends towards increased disease severity in female TNF-Tg mice for multiple parameters, yet only achieved significance in C_{rs} (C_{rs} female vs male, TNF-Tg, $p=0.0001$, rest of data not presented).

TNF-Tg mice have inflammatory cellular accumulation in interstitial tissue

We next wanted to compare how results obtained using comprehensive PFT's compared with non-invasive μCT. Similar to our previous studies (14), three-dimensional reconstructions for tissue volumes in all cohorts confirmed that TNF-Tg mice have a clear increase in lung tissue volume (LTV) compared to their WT counterparts (Red, Fig. 3A–D). Quantification of these volumes demonstrates that TNF-Tg mice have significantly greater tissue volumes compared to WT controls for both sexes (WT vs TNF-Tg, female, $p=0.0008$; male, $p<0.0001$)., yet no differences were found between the sexes (female vs male, WT, $p=0.9998$; TNF-Tg, $p=0.6673$) (Fig. 3I). Similar reconstructions of air volume and quantification show that the basal air volume at immediate post-exhalation in these mice have no significant differences with regard to genotype between the cohorts (WT vs TNF-Tg, female, $p=0.8815$; male, $p=0.3584$) (Fig. 3E–H, J). Remarkably, a sexual dimorphism was noted here regarding the TNF-Tg mice, with females having significantly decreased air volumes compared to the males ($p=0.0396$) (Fig. 3J).

Masson trichrome staining for collagen deposition was performed on representative slides from all cohorts to determine the possibility of fibrotic change in TNF-Tg mice. Interestingly, no signs of increased collagen deposition were found in diseased lungs (Fig. 3K–N). Instead, a dramatic cellular density in the interstitial tissue, and some cellular accumulation around vasculature, was found in all sections taken from TNF-Tg lungs. In a separate project, we characterized these cells by flow and found them to be inflammatory cells which were predominantly myeloid in nature based on their $CD11b^{+}CD11c^{+}$ nature (31).

Lung tissue volume is correlated to multiple physiologic parameters as determined by μCT and PFTs

Spearman's correlation analyses were performed comparing LTV (as determined by μCT), and multiple PFT outcome measures. LTV was significantly correlated to R_{rs} (rho=0.4842, p=0.0192, Fig. 4A), C_{rs} (rho=−0.6265, p=0.0014, Fig. 4B), and IC (rho=−0.5356, p=0.0084, Fig. 4C). All results are listed in Table 1. Note that when genotypes were analyzed independently, the correlations for tissue volume to each physiologic parameter were significantly weaker and were no longer significantly associated to each other for either genotype (data not shown). Spearman's correlations were also found to be significant between LTV and multiple other mechanical and functional parameters, including the DFCO (as determined by GC) and PFTs (Supplementary Fig. 1, Supplementary Table 1).

Discussion

The TNF-Tg mouse model of RA-ILD demonstrates an inflammatory pulmonary pathology that has been cited as demonstrating a mixture of restrictive and obstructive disease on histologic examination (26, 28, 29, 33–35). As the restrictive nature of clinical ILD puts into question the fitness of the TNF-Tg mouse as a relevant model, studies to resolve this controversy are warranted.

In this study, we performed comprehensive PFTs in the TNF-Tg model of inflammatory RA-ILD and compared these results with μCT imaging outcomes of quantified lung volumes and density. Most significantly, we found that: 1) the TNF-Tg mouse model demonstrates signs of restrictive disease over a number of physiologic parameters, and 2) all of the parameters found to be significantly different in diseased mice when compared to their WT counterparts were also found to be significantly correlated to LTV as measured by μCT. Female TNF-Tg mice consistently demonstrated decreased gas exchange functionality, while TNF-Tg mice of both sexes demonstrated changes in respiratory resistance, compliance, elasticity, and inspiratory capacity, all of which pointed towards restrictive pulmonary disease with increased tissue stiffness. Spearman's analyses associating the μCT-obtained tissue volumes and the mechanical parameters found significant correlations over multiple comparisons. Taken together, these results validate the TNF-Tg as a model of restrictive RA-ILD, and also suggest that cross-sectional μCT imaging is a useful correlative biomarker of pulmonary physiology for in vivo longitudinal studies of disease progression.

While differences in multiple pulmonary physiologic parameters were found in both sexes, the effects on the female cohorts are of greater magnitude, reflecting a functional sexual

dimorphism in the model which mimics the clinical demographics of RA. The sexual dimorphism of the TNF-Tg model has been noted in the context of both systemic symptoms and pulmonary manifestations (31). Placed in the context of clinical disparities, in which females present with greater prevalence and disease severity than male RA patients, these findings could have large implications regarding the role of sex hormones on disease pathogenesis. Future studies regarding the effects of hormone manipulation on pulmonary disease are warranted.

Describing pulmonary function as a primary outcome measure is a vital tool for tracking and assessing pulmonary disease progression in animal models; however, given the invasive nature of our current protocols for mechanical and functional testing in murine models, longitudinal studies assessing the same animals over the course of disease development is not a viable option. Our lab has previously developed an in vivo μCT imaging protocol for the assessment of murine lungs and validated it against histomorphometry outcome measures (14). μCT as a non-invasive imaging modality allows for the evaluation of pulmonary disease progression over time within the same animal, making it a tool of enormous potential for longitudinal study of progressive disease development; but this technique does not address all features of the lung. μCT certainly cannot directly measure the functional parameters of pulmonary physiology. However, given the reproducible and severe phenotype of the model, we hypothesized that changes in functional and mechanical properties of the pulmonary tissue would directly correlate with the severity of disease. The use of these longitudinal imaging methods could therefore be used as a correlative marker for pulmonary function and mechanical physiology.

TNF-α has previously been shown to cause pathologic changes in the lung (26, 28). We attribute the increased tissue stiffness and volume to the accumulation of a cellular infiltrate into the pulmonary interstitium (14, 26, 31). Histologic findings confirmed the presence of leukocytic accumulation and lack of collagen deposition, indicating an inflammatory rather than a fibrotic pathology. The findings here (Fig. 3K–N), and in previous publications (14, 26), suggest that this model is one of a predominantly inflammatory state. It should be noted that while the majority of patients with RA-ILD ultimately exhibit some form of fibrotic change in their pulmonary manifestations, we do not claim that this TNF-Tg model fully depicts all aspects of clinical disease. However, we propose it could be a useful model to elucidate the relationship between TNF-driven inflammation and the onset of interstitial lung disease.

Several limitations of this study and of the data must be considered when interpreting our results. First, we obtained μCT images using respiratory gating at the post-exhalation phase of the respiratory cycle. The primary purpose of our gating strategy, which involved a pressure transducer to monitor chest wall movement, was to reduce motion artifact in the imaging process. This served the purpose of monitoring large movements and estimating the respiratory cycle in real time. Due to the very nature of our μCT data collection methodology, the lung can only be imaged in the post-exhalation phase of the respiratory cycle. The air volume calculated here is most comparable to the functional residual capacity (FRC), which is defined as the volume of air at steady-state with no airflow into or out of the lungs. Interestingly, we found that air volumes as derived from the 3D μCT renderings were

not different between the two genotypes in age-matched animals. This is inconsistent with what would be considered typical, as FRC volumes are generally decreased in restrictive diseases. However, given the differences in respiratory mechanics and chest wall compliance between mice and humans (36), it is difficult to know how exactly μCT air volume obtained using this approach relates to lung volumes obtained during pulmonary function testing (including the FRC). Importantly, the inspiratory capacity, which we measured directly, was significantly reduced in TNF-Tg mice compared to wild-type controls.

The second issue, which should be addressed in later studies, is in regard to the correlation analyses when analyzing the data set within individual genotypes. While associations between μCT data and PFT data were significantly correlated (Figure 4), these correlations were largely driven by genotype-specific differences. The WT data was not expected to have a strong association, as these lungs were healthy, and all of the data clustered within a small range of variability for all factors; however, the TNF-Tg lungs demonstrated a greater range of variability with regard to disease severity and functional capacity. While trends could be seen for many of these analyses, none reached statistical significance within each genotype with our pooled dataset (n=12). This is most likely attributable to the fact that we surveyed the extreme ends of the disease spectrum, healthy controls compared to terminal pathology. In attempting to maintain low genetic, environmental, and batch-effect variability, this study used sets of age-matched (5.5 month-old) littermates to determine the physiologic changes of fully developed disease. While this provided much needed consistency in the data collection and definitively asserted the phenotype of the disease outcome, this inherently divided the results into a bimodal data set. In future studies, longitudinal data demonstrating progressive development of the pathology over time would produce a continuous distribution of the data, which would provide the range of disease severity necessary to perform more nuanced correlation analyses.

Finally, we previously noted that the TNF-Tg lungs demonstrated a purely inflammatory phenotype with no signs of interstitial fibrotic change, whereas clinical RA-ILD typically has some level of fibrotic activity. These results of non-fibrotic pathology in the systemic TNF-Tg model are also in contrast to some previously published findings regarding the pathology found in a local pulmonary TNF-Tg model. This local model is driven by the surfactant protein-C promoter (Sp-C/TNF-Tg), thereby expressing TNF-α selectively in the pulmonary tissue, and exhibits an lymphocytic inflammatory pathology that progresses to fibrosing alveolitis with signs of emphysematous change on histologic analysis, alongside interstitial collagen deposition (28, 29, 35). It should be noted that the locally expressed TNF-α model has never reported systemic effects outside of the lung, and the levels of TNF-α expression in the lungs have not been directly compared between the models. In the development and initial characterization of the model, Miyazaki et al describe multiple iterations carrying variable amounts of the TNF-transgene (29). This resulted in large variability in disease severity, with varying degrees of inflammation and widely divergent lifespans between individual mice. These mice progressed to terminal disease at times between <24 hours to 7 months of age, and demonstrated signs of hyperplasia, lymphocytic alveolitis, emphysematous change, and fibrosis. Lundblad et al, in their analysis of the Sp-C/TNF-Tg model, used animals which were aged 7–11 months, and therefore underwent much longer periods of disease progression than our systemic TNF-Tg model (28). As a more

chronic iteration of TNF-α effects on the lung, this fibrosis is described as diffuse, with the collagen depositions in septa and along the larger airways. While neither of the reports quantified the levels of collagen specifically in the interstitial spaces, representative images from each study show characteristically different phenotypes with regard to the magnitude of fibrotic activity and patterns of collagen deposition. It should be noted that other models of RA-ILD have demonstrated fibrotic change as part of their phenotypes. These include the SKG model, an inconsistent T cell-dependent model (37), and the adjuvant-induced arthritis model, which is a collagen-immunization model with inflammatory components (38, 39). Our current study only looked at preliminary histologic evidence of fibrotic activity using Masson's Trichrome staining. Further assays of collagen deposition and extracellular matrix production would be needed to comprehensively assess any sub-clinical fibrotic change in the pulmonary tissue. These would include hydroxyproline assays, along with Picosirius red staining, and Miller's elastic staining to assess both collagen and elastin deposition in the interstitial tissue. Future studies involving the induction of fibrosis in the model will serve to provide a more severe phenotype that has greater face validity with clinical disease. Although we cannot rule out the possibility that lung fibrosis occurred below the resolution of our histochemical staining, we have definitively shown that the systemic TNF-Tg mouse demonstrates restrictive physiology.

In conclusion, we have quantitatively determined that the TNF-Tg model of RA-ILD demonstrates a restrictive pulmonary pathology with regard to both mechanical and functional physiologic parameters. Pulmonary function testing revealed multiple outcome measures indicating significantly increased tissue "stiffness", with histologic evidence concluding that the pathology is predominantly inflammatory and non-fibrotic in nature. These parameters as found through comprehensive pulmonary function testing and analysis of lung gas exchange are also significantly correlated to LTV as determined by previously developed μCT imaging methods. Therefore, the TNF-Tg mouse model demonstrates a significant inflammatory pathology with restrictive physiology, and can provide insights into interstitial lung diseases that develop in patients with inflammatory diseases associated with TNF-α overproduction, such as rheumatoid arthritis.

Supplementary Material

Refer to Web version on PubMed Central for supplementary material.

Acknowledgements

The authors would like to thank Michael Thullen for help with the μCT imaging and analysis. This work was funded by grants from NIH MSTP T32 GM007356, NIH/NIAMS T32 AR053459, NIH/NIAMS P30 AR069655, NIH/NIAMS K08 AR067885, NIH/NIAMS R01 AR56702, and NIH/NHLBI R01 HL122424.

References

1. Assayag D, Lubin M, Lee JS, King TE, Collard HR, Ryerson CJ. Predictors of mortality in rheumatoid arthritis-related interstitial lung disease. Respirology 2014;19(4):493–500. [PubMed: 24372981]

2. Gabriel SE, Crowson CS, Kremers HM, Doran MF, Turesson C, O'Fallon WM, Matteson EL. Survival in rheumatoid arthritis: A population-based analysis of trends over 40 years. Arthritis Rheum 2003;48(1):54–58. [PubMed: 12528103]

3. Bongartz T, Nannini C, Medina-Velasquez YF, Achenbach SJ, Crowson CS, Ryu JH, Vassallo R, Gabriel SE, Matteson EL. Incidence and mortality of interstitial lung disease in rheumatoid arthritis: A population-based study. Arthritis Rheum 2010;62(6):1583–1591. [PubMed: 20155830]

4. Olson AL, Swigris JJ, Sprunger DB, Fischer A, Fernandez-Perez ER, Solomon J, Murphy J, Cohen M, Raghu G, Brown KK. Rheumatoid arthritis-interstitial lung disease-associated mortality. Am J Respir Crit Care Med 2011;183(3):372–378. [PubMed: 20851924]

5. Sparks JA, Chang SC, Liao KP, Lu B, Fine AR, Solomon DH, Costenbader KH, Karlson EW. Rheumatoid arthritis and mortality among women during 36 years of prospective follow-up: Results from the nurses' health study. Arthritis Care Res (Hoboken) 2016;68(6):753–762. [PubMed: 26473946]

6. Kim EJ, Collard HR, King TE Jr. Rheumatoid arthritis-associated interstitial lung disease: The relevance of histopathologic and radiographic pattern. Chest 2009;136(5):1397–1405. [PubMed: 19892679]

7. Kim EJ, Elicker BM, Maldonado F, Webb WR, Ryu JH, Van Uden JH, Lee JS, King TE Jr., Collard HR. Usual interstitial pneumonia in rheumatoid arthritis-associated interstitial lung disease. Eur Respir J 2010;35(6):1322–1328. [PubMed: 19996193]

8. Tanaka N, Kim JS, Newell JD, Brown KK, Cool CD, Meehan R, Emoto T, Matsumoto T, Lynch DA. Rheumatoid arthritis-related lung diseases: Ct findings. Radiology 2004;232(1):81–91. [PubMed: 15166329]

9. O'Dwyer DN, Armstrong ME, Cooke G, Dodd JD, Veale DJ, Donnelly SC. Rheumatoid arthritis (ra) associated interstitial lung disease (ild). Eur J Intern Med 2013;24(7):597–603. [PubMed: 23916467]

10. Luukkainen R, Saltyshev M, Pakkasela R, Nordqvist E, Huhtala H, Hakala M. Relationship of rheumatoid factor to lung diffusion capacity in smoking and non-smoking patients with rheumatoid arthritis. Scand J Rheumatol 1995;24(2):119–120. [PubMed: 7747143]

11. Lee HK, Kim DS, Yoo B, Seo JB, Rho JY, Colby TV, Kitaichi M. Histopathologic pattern and clinical features of rheumatoid arthritis-associated interstitial lung disease. Chest 2005;127(6): 2019–2027. [PubMed: 15947315]

12. Doyle TJ, Dellaripa PF. Lung manifestations in the rheumatic diseases. Chest 2017.

13. Travis WD, Costabel U, Hansell DM, King TE Jr., Lynch DA, Nicholson AG, Ryerson CJ, Ryu JH, Selman M, Wells AU, et al. An official american thoracic society/european respiratory society statement: Update of the international multidisciplinary classification of the idiopathic interstitial pneumonias. Am J Respir Crit Care Med 2013;188(6):733–748. [PubMed: 24032382]

14. Bell RD, Rudmann C, Wood RW, Schwarz EM, Rahimi H. Longitudinal micro-ct as an outcome measure of interstitial lung disease in tnf-transgenic mice. PLoS One 2018;13(1):e0190678. [PubMed: 29320550]

15. Rodt T, von Falck C, Dettmer S, Halter R, Maus R, Ask K, Kolb M, Gauldie J, Langer F, Hoy L, et al. Micro-computed tomography of pulmonary fibrosis in mice induced by adenoviral gene transfer of biologically active transforming growth factor-beta1. Respir Res 2010;11:181. [PubMed: 21176193]

16. De Langhe E, Vande Velde G, Hostens J, Himmelreich U, Nemery B, Luyten FP, Vanoirbeek J, Lories RJ. Quantification of lung fibrosis and emphysema in mice using automated micro-computed tomography. PLoS One 2012;7(8):e43123. [PubMed: 22912805]

17. Vande Velde G, Poelmans J, De Langhe E, Hillen A, Vanoirbeek J, Himmelreich U, Lories RJ. Longitudinal micro-ct provides biomarkers of lung disease that can be used to assess the effect of therapy in preclinical mouse models, and reveal compensatory changes in lung volume. Dis Model Mech 2016;9(1):91–98. [PubMed: 26563390]

18. Kelly CA, Saravanan V, Nisar M, Arthanari S, Woodhead FA, Price-Forbes AN, Dawson J, Sathi N, Ahmad Y, Koduri G, et al. Rheumatoid arthritis-related interstitial lung disease: Associations, prognostic factors and physiological and radiological characteristics--a large multicentre uk study. Rheumatology (Oxford) 2014;53(9):1676–1682. [PubMed: 24758887]

19. Solomon JJ, Chung JH, Cosgrove GP, Demoruelle MK, Fernandez-Perez ER, Fischer A, Frankel SK, Hobbs SB, Huie TJ, Ketzer J, et al. Predictors of mortality in rheumatoid arthritis-associated interstitial lung disease. Eur Respir J 2016;47(2):588–596. [PubMed: 26585429]
20. Meyer KC. Diagnosis and management of interstitial lung disease. Transl Respir Med 2014;2:4. [PubMed: 25505696]
21. Franquet T High-resolution ct of lung disease related to collagen vascular disease. Radiol Clin North Am 2001;39(6):1171–1187. [PubMed: 11699667]
22. Limjunyawong N, Fallica J, Ramakrishnan A, Datta K, Gabrielson M, Horton M, Mitzner W. Phenotyping mouse pulmonary function in vivo with the lung diffusing capacity. J Vis Exp 2015(95):e52216. [PubMed: 25590416]
23. Vanoirbeek JA, Rinaldi M, De Vooght V, Haenen S, Bobic S, Gayan-Ramirez G, Hoet PH, Verbeken E, Decramer M, Nemery B, et al. Noninvasive and invasive pulmonary function in mouse models of obstructive and restrictive respiratory diseases. Am J Respir Cell Mol Biol 2010;42(1):96–104. [PubMed: 19346316]
24. Keffer J, Probert L, Cazlaris H, Georgopoulos S, Kaslaris E, Kioussis D, Kollias G. Transgenic mice expressing human tumour necrosis factor: A predictive genetic model of arthritis. EMBO J 1991;10(13):4025–4031. [PubMed: 1721867]
25. Li P, Schwarz EM. The tnf-alpha transgenic mouse model of inflammatory arthritis. Springer Semin Immunopathol 2003;25(1):19–33. [PubMed: 12904889]
26. Bawadekar M, Gendron-Fitzpatrick A, Rebernick R, Shim D, Warner TF, Nicholas AP, Lundblad LK, Thompson PR, Shelef MA. Tumor necrosis factor alpha, citrullination, and peptidylarginine deiminase 4 in lung and joint inflammation. Arthritis Res Ther 2016;18(1):173. [PubMed: 27450561]
27. Wu E, Ambrosini RD, Kottmann RM, Ritchlin CT, Schwarz EM, Rahimi H. Reinterpreting evidence of rheumatoid arthritis-associated interstitial lung disease to understand etiology: What do we really know? Curr Rheumatol Rev;2019.
28. Lundblad LK, Thompson-Figueroa J, Leclair T, Sullivan MJ, Poynter ME, Irvin CG, Bates JH. Tumor necrosis factor-alpha overexpression in lung disease: A single cause behind a complex phenotype. Am J Respir Crit Care Med 2005;171(12):1363–1370. [PubMed: 15805183]
29. Miyazaki Y, Araki K, Vesin C, Garcia I, Kapanci Y, Whitsett JA, Piguet PF, Vassalli P. Expression of a tumor necrosis factor-alpha transgene in murine lung causes lymphocytic and fibrosing alveolitis. A mouse model of progressive pulmonary fibrosis. J Clin Invest 1995;96(1):250–259. [PubMed: 7542280]
30. Fallica J, Das S, Horton M, Mitzner W. Application of carbon monoxide diffusing capacity in the mouse lung. J Appl Physiol (1985) 2011;110(5):1455–1459. [PubMed: 21310888]
31. Bell RD, Wu EK, Rudmann CA, Forney M, Kaiser CRW, Wood RW, Chakkalakal JV, Paris ND, Klose A, Xiao GQ, et al. Selective sexual dimorphism in musculoskeletal-cardiopulmonary pathologies and mortality in the tnf-transgenic mouse model of rheumatoid arthritis. Arthritis & Rheumatology 2019;In Press.
32. Hantos Z, Daroczy B, Suki B, Nagy S, Fredberg JJ. Input impedance and peripheral inhomogeneity of dog lungs. J Appl Physiol (1985) 1992;72(1):168–178. [PubMed: 1537711]
33. Fujita M, Shannon JM, Morikawa O, Gauldie J, Hara N, Mason RJ. Overexpression of tumor necrosis factor-alpha diminishes pulmonary fibrosis induced by bleomycin or transforming growth factor-beta. Am J Respir Cell Mol Biol 2003;29(6):669–676. [PubMed: 12816730]
34. Thomson EM, Williams A, Yauk CL, Vincent R. Overexpression of tumor necrosis factor-alpha in the lungs alters immune response, matrix remodeling, and repair and maintenance pathways. Am J Pathol 2012;180(4):1413–1430. [PubMed: 22322299]
35. Vuillemenot BR, Rodriguez JF, Hoyle GW. Lymphoid tissue and emphysema in the lungs of transgenic mice inducibly expressing tumor necrosis factor-alpha. Am J Respir Cell Mol Biol 2004;30(4):438–448. [PubMed: 12972399]
36. Irvin CG, Bates JH. Measuring the lung function in the mouse: The challenge of size. Respir Res 2003;4:4. [PubMed: 12783622]

37. Keith RC, Powers JL, Redente EF, Sergew A, Martin RJ, Gizinski A, Holers VM, Sakaguchi S, Riches DW. A novel model of rheumatoid arthritis-associated interstitial lung disease in skg mice. Exp Lung Res 2012;38(2):55–66. [PubMed: 22185348]

38. Song LN, Kong XD, Wang HJ, Zhan LB. Establishment of a rat adjuvant arthritis-interstitial lung disease model. Biomed Res Int 2016;2016:2970783.

39. Schurgers E, Mertens F, Vanoirbeek JA, Put S, Mitera T, De Langhe E, Billiau A, Hoet PH, Nemery B, Verbeken E, et al. Pulmonary inflammation in mice with collagen-induced arthritis is conditioned by complete freund's adjuvant and regulated by endogenous ifn-gamma. Eur J Immunol 2012;42(12):3223–3234. [PubMed: 22930199]

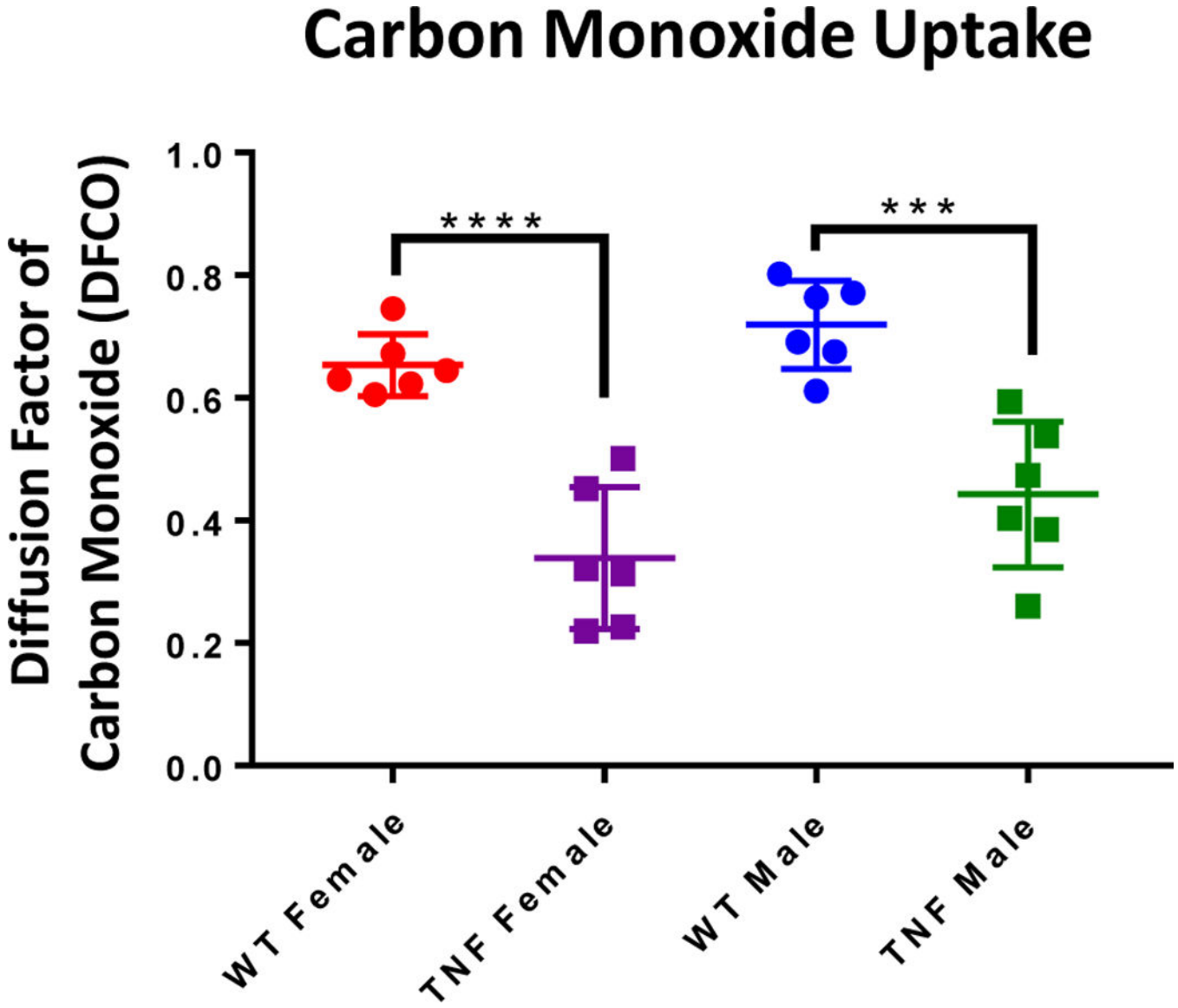

Figure 1. Gas exchange deficiency in TNF-Tg mice versus WT littermates.

5.5-month-old TNF-Tg male and female mice and their WT littermates underwent carbon monoxide (CO) diffusion testing as described in Materials and Methods. The relative abundance of CO post-expiration is presented as the diffusion factor of CO (DFCO) for individual mice with the mean +/− SD (n=6; ***p<0.001, ****p<0.0001). Analysis of differences between sexes within genotype were analyzed and found to not be significant (female vs male, WT, p=0.4205; TNF-Tg, p=0.1362).

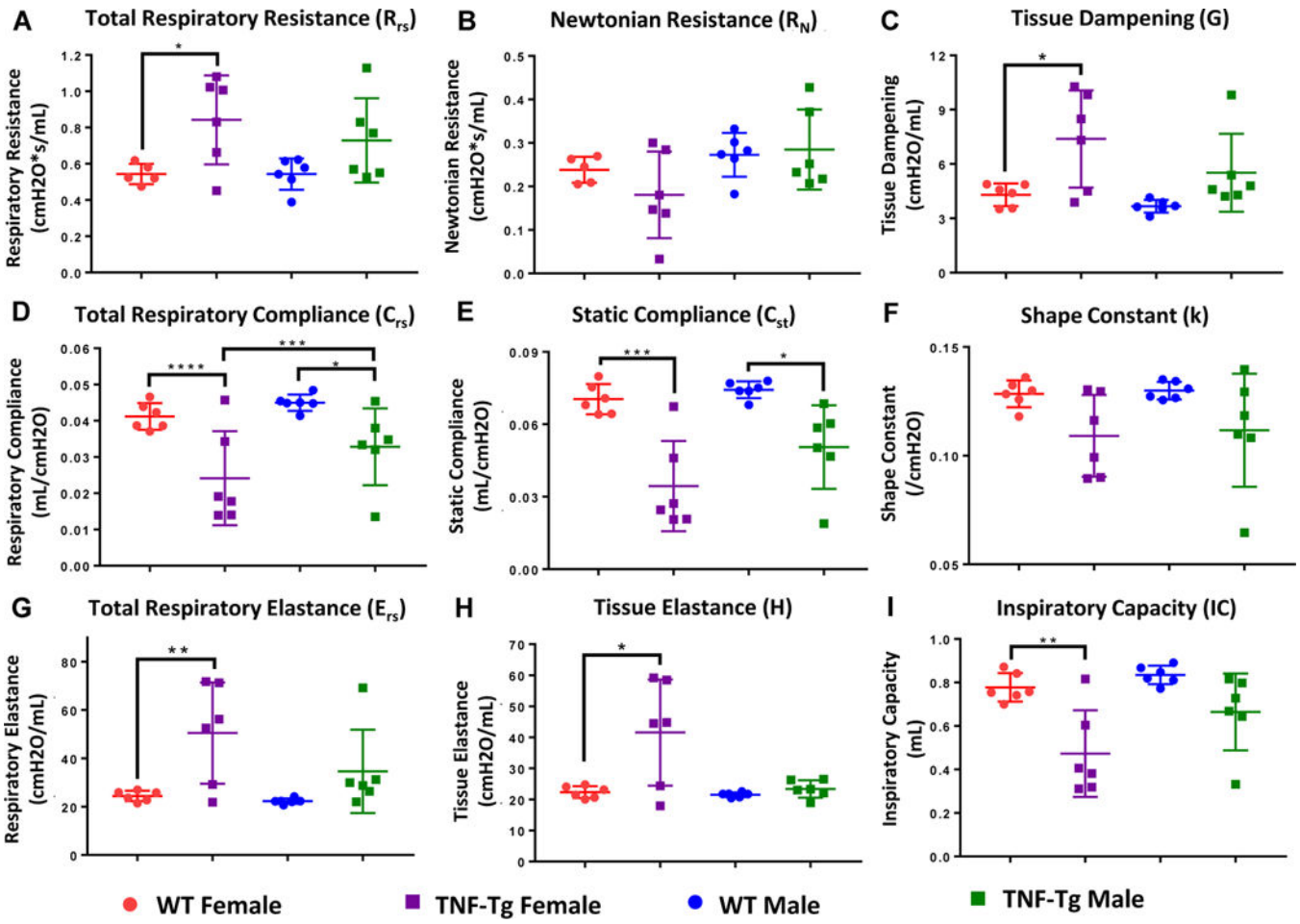

Figure 2. TNF-Tg lungs have a restrictive pulmonary pathology.

The mice described in Figure 1 underwent forced pulmonary manipulation as described in Materials and Methods. 2-way ANOVAs with Sidak's post hoc multiple comparisons were used to analyze differences in mechanical parameters between cohorts. Data for mechanical parameters: (A) total respiratory resistance, (B) Newtonian resistance, (C) tissue dampening, (D) total respiratory compliance, (E) static compliance, (F) the shape constant, (G) total respiratory elastance, (H) and tissue elastance, are presented for individual mice with mean +/− SD (n=6, *p>0.05,**p<0.01, ***p<0.001, ****p<0.0001). Note that within sex, differences between TNF-Tg and WT mice were found for multiple parameters measuring tissue "stiffness", including total respiratory resistance, tissue dampening, total respiratory compliance, static compliance, total respiratory elastance, and tissue elastance. Between the sexes, female TNF-Tg mice consistently trended towards increased disease severity compared to their male counterparts over multiple measures, yet only respiratory compliance reached statistical significance.

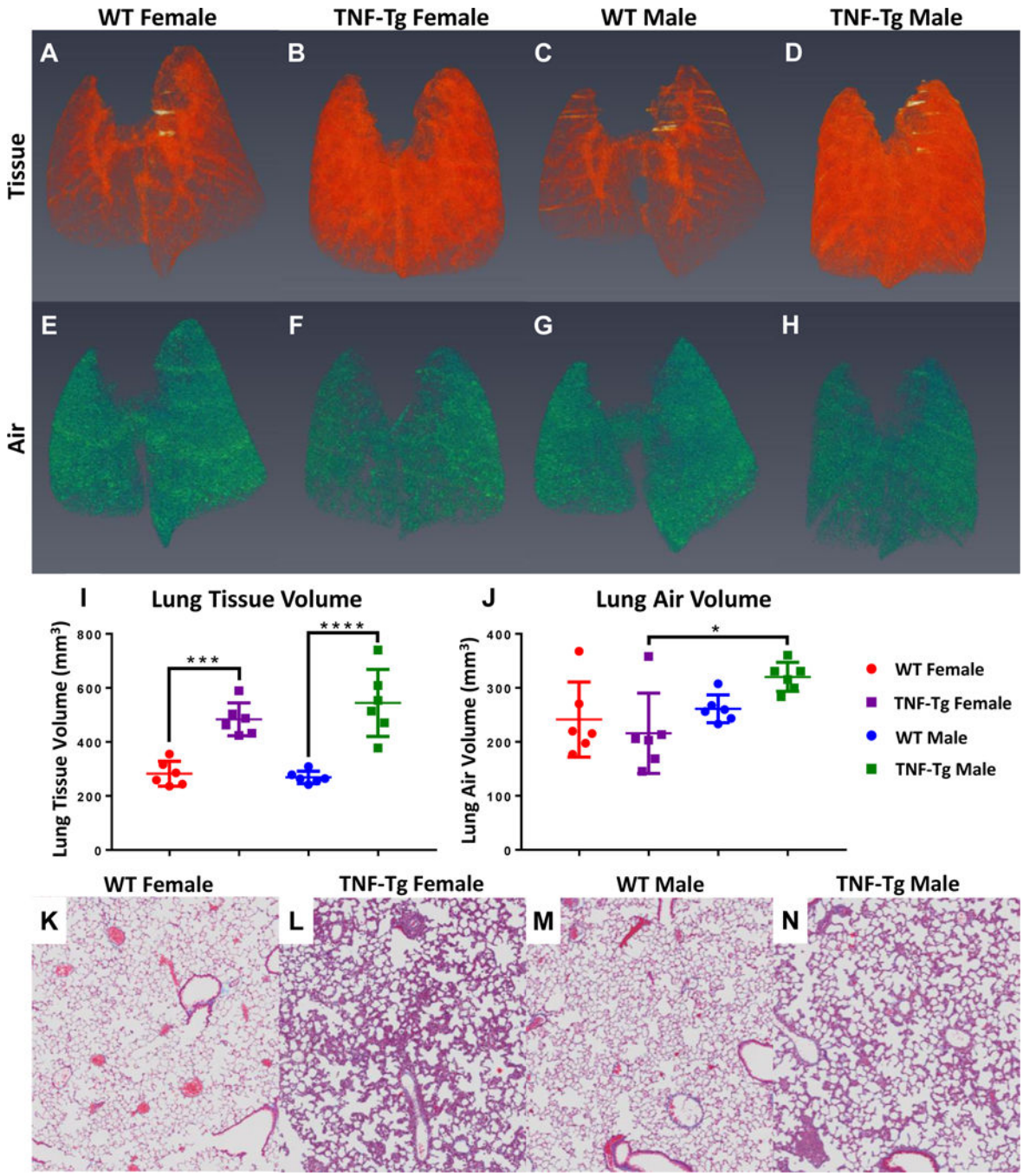

Figure 3. Radiographic and histologic confirmation of inflammatory ILD in TNF-Tg mice versus WT littermates.

The mice described in Figure 1 underwent in vivo micro-CT and ex vivo histopathology as described in Materials and Methods. Representative 3D renderings of lung tissue volume (A-D) and lung air volume (E-H) are presented with statistical analyses. Note that TNF-Tg mice have increased lung tissue volumes (I), while maintaining a comparable basal post-expiratory air volume (J) (n=6, mean +/− SD, *p>0.05, ***p<0.001, ****p<0.0001). Histologic sections stained with Masson's trichrome are shown to illustrate the absence of collagen deposition (blue tissue) in the interstitium of all mice (K-N). Histologic analysis

demonstrates marked inflammatory ILD in TNF-Tg mice versus their WT littermates (K-N). Note that the TNF-Tg male mice have lower cellular density by percent of total area than females, as determined through histology.

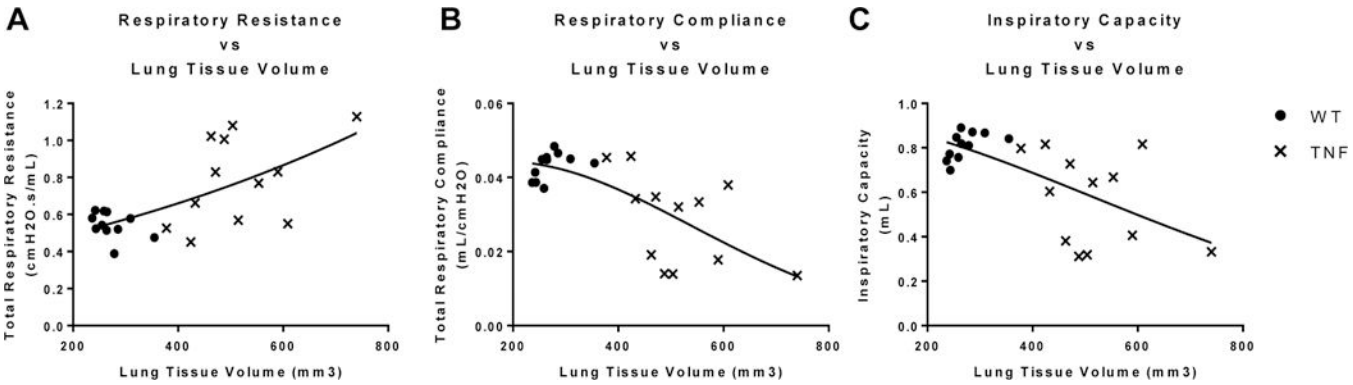

Figure 4. Correlation of pulmonary tissue physiology outcome measures with lung tissue volume.

Spearman's correlations were performed comparing the PFT outcome data in Figure 2 with the micro-CT lung volume data in Figure 3. The statistical findings are presented in Table 1. Graphs with best fit non-linear regression curves are presented to illustrate the relative correlation between lung volume and: Total Respiratory Resistance (A), Total Respiratory Compliance (B), and Inspiratory Capacity (C). ● = WT, x = TNF-Tg, n=12 per genotype.

Table 1.

Associations between pulmonary tissue physiology outcome measures and lung tissue volume as determined by in vivo micro-CT.

PFT and micro-CT data for all 24 mice in this study were combined for non-linear correlation analyses of Total Respiratory Resistance (R_{rs}), Total Respiratory Compliance (C_{rs}), and Inspiratory Capacity (IC). Spearman's correlations for each set of parameters are listed for all data points.

	Tissue Volume vs R_{rs}	Tissue Volume vs C_{rs}	Tissue Volume vs IC
R^2 (Non-Linear Fit)	0.4256	0.526	0.4382
Spearman's Correlation (Rho)	0.4842	−0.6265	−0.5356
Spearman's p value	0.0192	0.0014	0.0084
Significance	*	**	**

* $p<0.05$,

** $p<0.01$